Formation Mechanism of Colloidal Silver Nanoparticles: Analogies and Differences to the Growth of Gold Nanoparticles

Jörg Polte,[†,‡,§,*] Xenia Tuaev,[‡] Maria Wuithschick,[§] Anna Fischer,[‡] Andreas F. Thuenemann,[†] Klaus Rademann,[§] Ralph Kraehnert,[‡] and Franziska Emmerling[†,*]

[†]BAM Federal Institute of Materials Research and Testing, Richard-Willstätter-Strasse 11, D-12489 Berlin, Germany, [‡]Technical Chemistry, Technical University Berlin, Strasse des 17. Juni 124, D-10623 Berlin, Germany, and [§]Department of Chemistry, Humboldt University Berlin, Brook-Taylor-Str. 2, D-12489 Berlin, Germany

Metallic nanoparticles are of great interest due to their unique properties and numerous promising applications.[1,2] Though synthetic procedures are well-known and have been investigated since Faraday's pioneering work on gold sols more than 150 years ago,[3] a deeper understanding of the underlying nanoparticle formation processes is still missing. This is primarily caused by the absence of reliable experimental information on the actual size evolution and concentration of nanoparticles during the growth process.[4]

In general, descriptions of particle growth rely on the classical nanoparticle growth model of LaMer (from the 1950s) which is based on the classical nucleation theory developed by Becker and Döring in the 1930s. The central aspect of LaMer's model is that, after a discrete nucleation period due to a supersaturation, particles form during a growth process (*e.g.*, by monomer addition).[5] However, it has been intensively discussed if such a model of particle formation (based on the concept of nucleation) is able to describe particle growth or even predict particle size distributions.[6,7] Several studies have already shown that classical nucleation theory and its transfer to nanoparticles by LaMer can hardly explain their experimental results.[8−10] Summarizing, there is consensus that reliable experimental information which allows monitoring particle growth *in situ* and time-resolved is needed to determine fundamental principles of nanoparticle growth.

Recently, we showed that small-angle X-ray scattering (SAXS) is one of the most powerful techniques for time-resolved *in situ* investigations of nanoparticle growth

ABSTRACT
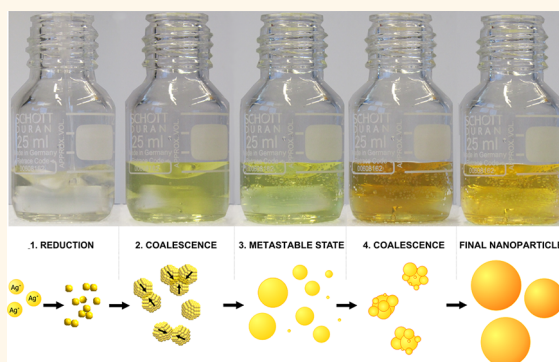
The formation mechanisms of silver nanoparticles using aqueous silver perchlorate solutions as precursors and sodium borohydride as reducing agent were investigated based on time-resolved *in situ* experiments. This contribution addresses two important issues in colloidal science: (i) differences and analogies between growth processes of different metals such as gold and silver and (ii) the influence of a steric stabilizing agent on the growth process. The results reveal that a growth due to coalescence is a fundamental growth principle if the monomer-supplying chemical reaction is faster than the actual particle formation.

processes since the method delivers this long demanded information.[11−14] As an example, common gold nanoparticle (Au-NP) syntheses were investigated. For each of the synthetic routes, a comprehensive growth mechanism could be deduced. When a continuous flow setup combined with SAXS was applied, it was shown that the growth process of a Au-NP synthesis based on the reduction of HAuCl$_4$ with NaBH$_4$ proceeds in two steps.[14] The first step is the initial and rapid reduction of the metal precursor (HAuCl$_4$) within less

than 200 ms, accompanied by the formation of small clusters (1 nm). In a second step, these small clusters grow due to coalescence, along with a corresponding decrease in the number of particles. In the experimentally accessible time frame, particle growth in the studied system is driven only by coalescence. This growth occurs on a time scale of a few seconds.

The aim of this work is to apply the knowledge gained by time-resolved *in situ* studies of Au-NPs to another metallic system, namely, silver nanoparticles (Ag-NPs). The investigation of the growth process of two Ag-NP syntheses is presented, applying time-resolved *in situ* SAXS and UV−vis studies, combined with conventional electron microscopy. Both syntheses comprise the same Ag precursor (aqueous silver perchlorate solution, $AgClO_4$) and reducing agent (aqueous sodium borohydride solution, $NaBH_4$). The first synthesis (denoted as Ag-System 1) was carried out without an additional stabilizing agent, whereas for the second system, polyvinylpyrrolidone (PVP) was used as steric stabilizing agent (denoted as Ag-System 2). Ag-System 1 was adapted from the work of Van Hyning and Zukoski, who first described this synthesis.[15−17] It is shown how PVP introduced as a steric stabilizing agent affects the growth mechanism and produces reliably monodisperse Ag-NPs ($\sigma = 10-15\%$).

These experiments are of vital interest in colloidal science since the results allow to address two important issues: (i) the differences and analogies between growth processes of different elements such as gold and silver and (ii) the influence of a steric stabilizing agent on the growth process. In fact, the influence of the stabilizing agent on the growth itself is in general unknown, especially for steric stabilizers such as the commonly chosen polymers.[18,19]

Additionally, detailed insights into the Ag-NP growth process might promote synthetic procedures for Ag-NPs with precise control of the size distribution.

RESULTS AND DISCUSSION

Important Processes and Their Nomenclature. In the following, important terms and processes of nanoparticle formation used in this contribution are explained to prevent misunderstanding since for different processes often the same term is used (*e.g.*, aggregation *vs* agglomeration). Some terms are defined according to the ISO Standard 27687 dealing with terminology in nanotechnology.[20] The terms agglomeration and aggregation are both characterizing an accumulation of objects comprising different types of bonding between these objects. In the case of nanoparticles, both terms describe a process that is mass-conserving but number-reducing and shifts the particle distribution toward larger sizes.

In the ISO Standard 2768712, agglomeration is defined as a "collection of weakly bound particles or aggregates or mixtures of the two where the resulting external surface area is similar to the sum of the surface
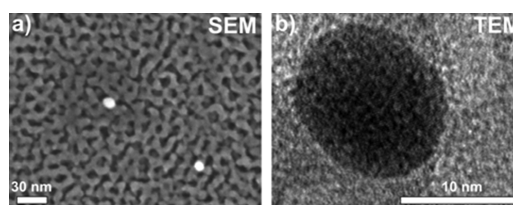

Figure 1. (a) SEM and **(b)** TEM image of the final colloids from Ag-System 1 spin-coated on a silicon wafer and TEM grid. The silicon wafer used for SEM measurements is coated with a mesoporous TiO_2 layer.

areas of the individual components. The forces holding an agglomerate together are weak forces, for example van der Waals forces, or simple physical entanglement."

The term aggregation is described as "comprising strongly bonded or fused particles where the resulting external surface area may be significantly smaller than the sum of calculated surface areas of the individual components. The forces holding an aggregate together are strong forces, for example covalent bonds, or those resulting from sintering or complex physical entanglement."

Coalescence is defined in the IUPAC Compendium of Chemical Terminology as a "process in which two phase domains of essentially identical composition in contact with one another form a larger phase domain. Coalescence reduces the total interfacial area."[20] Thus, coalescence can be understood as a merging of formed aggregates. Consequently, coalescence demands at first a process of aggregation.

Ag-System 1: Reduction of Silver Perchlorate Using Sodium Borohydride. The synthesis introduced by Van Hyning and Zukoski is based on the reduction of silver perchlorate ($AgClO_4$) with sodium borohydride ($NaBH_4$). They obtained spherical Ag-NPs with mean radii between 5 and 15 nm by varying reaction conditions (mainly concentrations of the reactants and the temperature).[17] However, the final nanoparticle size could not be controlled in a way to achieve particles with a certain size and a relatively low polydispersity. The authors proposed a nanoparticle growth due to an aggregation of small primary particles with diameters of 2−3 nm. The deduced mechanism is based on a temporary stabilization of small Ag-NPs by BH_4^- species. The collapse of the stabilization that causes the aggregation is attributed to the consumption of BH_4^- accompanied by hydrogen evolution:

$$BH_4^- + 4H_2O \rightarrow B(OH)_4^- + 4H_2$$
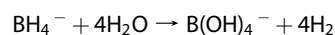
This interpretation of the growth process was derived by investigating the synthetic procedure with time-resolved *in situ* methods such as UV−vis spectroscopy and *ex situ* methods such as electron microscopy.

For the present study, the synthesis was adjusted to obtain a 1:1 mixing of the aqueous $AgClO_4$ (0.5 mM) and $NaBH_4$ (3 mM) solution, necessary for the used experimental setups and for a better handling. Further
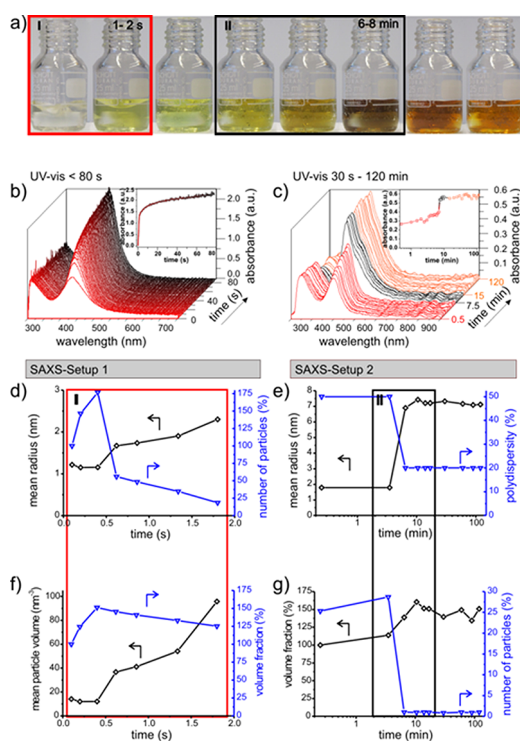
Figure 2. Photographs, UV−vis, and SAXS data of the early (b,d,f) and late stages (c,e,g) of the silver nanoparticle formation (Ag-System 1): (a) selected photographs of the colloidal solution during the synthesis; (b) UV−vis spectra recorded during Ag-NP formation in the first 80 s and (c) between 30 s and 120 min with the absorbance maximum as inset; (d) mean radius and number of particles (normalized to 1 at the last data point) plotted *vs* reaction time derived from SAXS with continuous flow setup (CFS) in the first 2 s of the reaction; (e) mean radius and polydispersity plotted *vs* reaction time derived from standard SAXS measurements; (f) mean particle volume and volume fraction (normalized to 100 at the first data point) *vs* reaction time derived from SAXS with a CFS in the first 2 s of the reaction; (g) volume fraction (normalized to 100 at the first data point) and number of particles (normalized to 1 at the last data point) *vs* reaction time derived from standard SAXS measurements.

details on the synthesis can be found in the Experimental Section. After mixing both solutions, within 1 s, the color turns from a transparent colorless solution into a transparent gray-yellow solution and within the next 1−5 s into a transparent bright-yellow solution. In the following 5 min, the color does not change considerably. Between 6 and 10 min, the color of the solution changes, from yellow to yellow-gray and subsequently to yellow-orange (see Figure 2a). This last step takes about 30 s. The yellow-orange color represents the final colloidal solution. The solution has to be stirred continuously throughout the reaction; otherwise, agglomeration of nanoparticles or precipitation of silver is observed. The long-term stability in terms of days, or even months, was not investigated, but the final colloidal solutions showed no changes after several days. The evaluation of the SAXS scattering curves showed that the final Ag-NPs have mean radii of 5−8 nm at polydispersities between 20 and

30%. A reproducibility study can be found in the Supporting Information (see S1).

The final nanoparticles of Ag-System 1 were investigated with SEM and TEM. In both cases, the samples had to be prepared by spin-coating the colloidal solution on the SEM wafer and TEM grid (wafer and grid were fixed and spun at around 10 000 rpm). Simple drying resulted in large aggregates on the wafer/grid surface, which impeded any size determination (for details, see Supporting Information S2). However, the few single particles which can be identified in these images show spherical shape sizes between 5 and 10 nm in radius. Figure 1 shows a representative SEM and TEM image that reveals spherical particles with radii of around 7 nm.

In Figure 2b,c, the results of different time-resolved *in situ* UV−vis experiments are displayed. The growth in the first minute was investigated by conducting the synthesis under stirring in a UV−vis cuvette (see Figure 2b). In the first 2 s, the absorbance around 390 nm increases rapidly up to 1.5 (see inset of Figure 2b), which shows the growth of Ag-NPs with radii between 2 and 15 nm.[21−23] A reliable size determination/approximation due to the position of the plasmon band is only possible for Ag-NPs having radii above 15 nm.[21−23] In the following minute, the particle growth decelerates and the absorbance increases slowly to about 2.5. This is in accordance with the color change of the reaction solution that immediately turns from colorless into gray-yellow after mixing the solutions and within further 5 s into bright-yellow.

A longer measurement period than the presented 80 s was not possible in the UV−vis cuvette due to the production of hydrogen, causing the formation of gas bubbles at the cuvette surface. Consequently, the subsequent growth was investigated with single UV−vis measurements by extracting successively small amounts of the solution from the reaction vessel. The sample was diluted with an aqueous solution of PVP (6.5×10^{-4} mM) in a 1:4 ratio (for details, see Experimental Section). Later in this contribution (Ag-System 2), it is shown that at reaction times of less than 30 min the synthesis can be decelerated using PVP as a steric stabilizer. The time delay between the extraction and the actual measurement was always less than 5 s.

The time evolution of the revealed absorption spectra recorded at reaction times between 30 s and 120 min and the corresponding absorbance maximum are displayed in Figure 2c. The inset shows that the slow increase of the absorbance maximum observed in the first 80 s of the reaction is continuous for further 5 min. Between 6 and 8 min, the spectrum changes remarkably. Within 20−30 s, the absorbance maximum increases from 0.4 to 0.6. This point in the reaction/synthesis will be referred as the "switching point".

The changing UV−vis spectrum corresponds to the color change from yellow to yellow-gray and

subsequently to a yellow-orange (see Figure 2a, box II). Afterward, the UV–vis spectrum does not show any changes.

Detailed information about the growth process can be gained by time-resolved *in situ* SAXS investigations since essential information, such as the particle size and concentration, is available.[11−14,24,25] However, the major experimental problem for time-resolved *in situ* SAXS investigations of Ag-System 1 is the need to stir the solution throughout the synthesis. As a result, precipitation, aggregation, or agglomeration of particles occurs during the measurement using standard sample holders such as quartz capillaries or unusual ones like an ultrasonic levitator or a free-liquid jet.[11−13] Nevertheless, the initial phase of particle formation between 200 ms and 2 s of the reaction (see Figure 2a, box I) could be investigated with the continuous-flow setup (CFS, SAXS setup 1 described in the Experimental Section), which we recently introduced for the investigation of the corresponding Au-NP growth process.[14] The subsequent growth was investigated with SAXS by quenching the growth by adding PVP and suppressing agglomeration for a certain amount of time (SAXS setup 2 described in the Experimental Section). This procedure is similar to the UV–vis measurement.

The results of the SAXS study using the CFS (first 2 s) are shown in Figure 2d,f. From each scattering curve, the mean radius and particle volume (d), polydispersity (constant at 50%), relative volume fraction (directly proportional to the total volume of all particles) (f). and relative number of particles (d) is available. The size distribution is assumed to be a Schulz-Zimm distribution. which is shown to be a suitable but also necessary approximation.[13] Selected scattering curves and their corresponding theoretical fits are shown in Figure S3a (Supporting Information; details of the mathematical evaluation of the scattering curves are presented in the Experimental Section). The radius/number of particles *versus* time (Figure 2d) and the mean particle volume/ volume fraction *versus* time (Figure 2f) are displayed. At all stages of the growth process, the polydispersity was constantly high around 50% and therefore kept constant (at 50%) for the mathematical modeling.

Within the first 100 ms, the formation of particles with a mean radius of approximately 1 nm is observed (Figure 2d). This particle radius is close to the resolution limit of common lab-scale SAXS instruments. In the following 300 ms, the mean radius remains constant but the number of particles and thus also the volume fraction (embodies the whole volume of all particles) increase by around 40%. In the following 2 s, the particles grow to a size of 2.3 nm in radius, accompanied by a decrease in the number of particles (Figure 2d). In the same period of time, the mean particle volume increases considerably. In contrast, the volume fraction remains almost constant (slight decrease of 20%). Assuming that the radial electron

density of a Ag-NP is constant upon growth in radius from about 1 to 2.3 nm, the number of particles decreases when the particles grow in size. Interestingly, these results of the initial growth stage are similar to the corresponding Au-NP experiment whereby $HAuCl_4$ is reduced by $NaBH_4$ at similar concentrations.[14] It was shown that the growth of the Au-NPs is only due to coalescence. A major difference in the present system is the slightly increasing volume fraction in the first 400 ms, which can be interpreted in different ways. Assuming that the whole amount of silver ions is reduced within the first 100 ms (as it is the case for the Au-NP system), the polydispersity might be higher than 50%. One has to keep in mind that particles smaller than 1 nm in diameter are hardly detectable due to the relative low signal-to-noise ratio of the lab experiments but also due to the resolution limit of SAXS with respect to the particle size (diameter <1 nm). Therefore, the actual increase of the volume fraction could be a consequence of the limitations of the SAXS method, in particular, for a lab-scale instrument. Nevertheless, it cannot be excluded that the reduction of $AgClO_4$ is much slower than of $HAuCl_4$ and the increase of the volume fraction is related to the reduction rate. However, a slow reduction would be counterintuitive since $NaBH_4$ is a relatively strong reducing agent. The concentrations are almost the same as for the corresponding Au-NP synthesis, and the redox potentials (Ag^+/Ag and Au^{3+}/Au) are comparable. Furthermore, Van Hyning *et al.* proved experimentally that within the first seconds no ionic silver remains in the reaction solution. Thus, it is most likely that the precursor is completely reduced within the mixing time (few milliseconds).

The actual particle growth is always accompanied by a commensurate decrease of the number of particles. The further particle growth was investigated with a standard SAXS laboratory setup (SAXS setup 2 described in the Experimental Section) using a quartz capillary, by extracting samples from the batch and mixing them with PVP dissolved in water. Selected scattering curves and their corresponding theoretical fits are shown in Figure S3b (Supporting Information). The results of the SAXS study are displayed in Figure 2e,g (radius/polydispersity *vs* time and volume fraction/number of particles *vs* time). A remarkable change at the switching point (SP) around 6−8 min can also be observed from the UV–vis. Before the SP-1, the Ag-NPs have a relatively high polydispersity (50%) at a mean radius of around 2 nm. After the SP-1, the mean radius increases to around 6 nm at a much lower polydispersity (20%). The particle growth is accompanied by a considerable decrease of the particle concentration, by a factor of around 30 (final value of the number of particles is normalized to 1). The volume fraction increases at the SP-1 by almost 50%. This indicates the existence of smaller particles (diameter <1 nm) that are not detected in the presence of larger
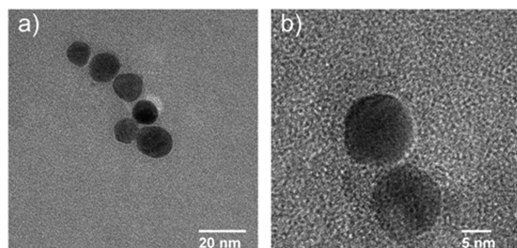
**Figure 3. Representative TEM images of the final particles from Ag-System 2.**

particles (radius >1 nm) before the SP. This observation is similar to the increase of the volume fraction in the first 400 ms of the CFS experiment. Consequently, the polydispersity might be significantly higher than the 50%. As a result, the increase of the volume fraction in the first 5–6 min is caused by a slow growth of smaller particles. This is in agreement with the slight increase of the absorbance maximum (see Figure 2b,c).

A more precise determination of very high polydispersities (as in the beginning of the synthesis) is in general difficult to determine with SAXS since the scattering intensity scales with the sixth power of the radius but would in any case demand a better signal-to-noise ratio.

Nanoparticle Growth Mechanism Deduced for Ag-System 1. According to the experimental results, the particle growth mechanism can be divided into four steps, as displayed in Figure 6. It has to be noted that this mechanism is different from the four-step mechanism deduced for the classical citrate synthesis of Au-NPs.[11] The initial step is the rapid reduction of the silver precursor. In a second step, these reduced metal atoms form dimers, trimers, *etc.* These clusters/nanoparticles coalesce further until the particles have a certain stability that stops the process of coalescence. This can be deduced from the decreasing particle concentration. These two steps occur within the first 5 s (see Figure 2a,b,d,f), after which the particles have a size of around 2–3 nm in radius. The third step describes an intermediate phase of stability in which particles larger than 1 nm are not growing in radius anymore. At a certain point of the synthesis (the switching point), the colloidal stability decreases abruptly. This change induces a further growth due to coalescence and eventually produces particles with mean radii between 5 and 8 nm. This comprises the fourth (final) step of the synthesis. After this fourth step, the particles are stable in terms of days and the solution does not need to be stirred anymore.

Summarizing, the growth mechanism of Ag-System 1 is only due to coalescence but separated in two distinct processes. The growth mechanism is governed by the electrostatic stabilization of the particles. Hence, after adding a steric stabilizer to the system, the growth must change due to the effect on the particle stability. Furthermore, an investigation of the growth process
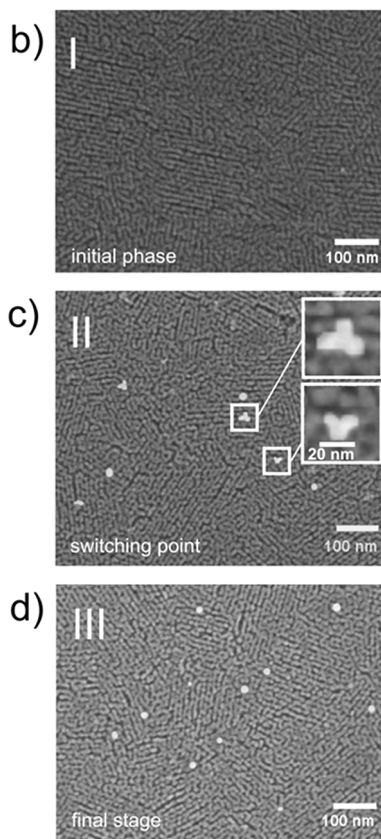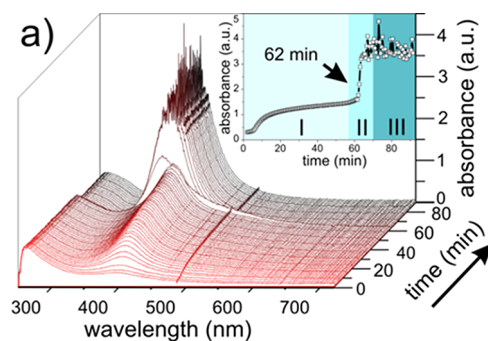
Figure 4. UV–vis and SEM data on the formation of silver nanoparticles (Ag-System 2): (a) UV–vis spectra recorded during the Ag-NP formation. The inset shows the intensity of plasmon resonance band at the band maximum. (b) SEM image of initial phase of the synthesis, (c) at the switching point, and (d) after completed synthesis (final particles).

should yield information of how the steric stabilizing agent affects the growth process.

Ag-System 2: Reduction of Silver Perchlorate Using Sodium Borohydride and an Additional Steric Stabilizing Agent (PVP). Adding a further stabilizing agent (PVP) to the beforehand described synthesis reveals spherical particles with mean radii between 5 and 7 nm at lower polydispersities between 10 and 20%. Again, the synthesis was investigated with TEM, SEM, UV–vis, and SAXS.

In Figure 3, representative TEM images of the final particles are displayed. The TEM images show spherical particles with radii of around 5–7 nm. A size determination of the final nanoparticles using SEM, TEM, and SAXS can be found in the Supporting Information

(see S4). For a specific sample all three methods reveal a mean radius of about 5 nm.

Similar to the procedure described for Ag-System 1, UV—vis absorption spectra were collected *in situ* and time-resolved to determine the kinetics of the Ag-NP formation and to correlate the optical properties with the size of the nanoparticles derived from the SAXS experiments. The whole synthesis was carried out in a standard UV—vis cuvette with a volume of 1 mL. The absorption spectra of time-resolved UV—vis measurements from several experiments show a similar chronological behavior, as shown in Figure 4a. At a certain point, the absorbance increases rapidly (see Figure 4a), which is again referred to as the switching point (SP-2). After this SP-2, which occurs between 30 and 90 min, the plasmon resonance does not change anymore.

The evolution of the absorbance at around 390 nm (SP-2 at 62 min) is shown in the inset of Figure 4a. Samples of the solution at three different stages of the reaction (after 5 min, at the SP-2, and after the completeness of the growth) were extracted for a SEM analysis. The colloidal solutions were deposited on a SEM wafer (mesoporous titania-coated Si wafers) *via* spin-coating. The preparation procedure was chosen to minimize an aging of the Ag-NPs during the drying process of the solution to avoid aggregation and to minimize the deposition of the polymer.

The drying process/sample preparation lasted less than 2 s. SEM images are shown in Figure 4b—d. A few minutes after mixing the solution, no particles are detectable on the wafer surface (see Figure 4b), most likely due to their small size (<1—2 nm in radius). At the SP-2 (see Figure 4c), spherical particles with radii of about 3—4 nm are visible among several aggregated particles. It remains unclear whether this is a drying artifact or represents the condition of the particles in solution. However, aggregated nanoparticles were only found on SEM images obtained from samples prepared during the SP-2.

According to the results of the UV—vis measurements, the final size of the particles is reached after the SP-2. The SEM image displays the final Ag-NPs (see Figure 4d) having a spherical shape and an average radius of 5—6 nm.

The results of UV—vis, SEM, and TEM reveal a slow growth process in the first 30—90 min of the reaction followed by a sudden change at the SP-2. Subsequently, the growth process is finished. A more detailed view on the growth can be gained by *in situ* and time-resolved SAXS measurements. A major issue for such experiments is the need to stir the solution throughout the synthesis. However, in contrast to Ag-System 1, the colloids do not aggregate/agglomerate for at least 5 min when samples are extracted before the SP. The addition of PVP preserves the state of the colloidal solution without stirring for more than a minute.

Therefore, the SAXS measurements could be conducted using a free liquid jet at a synchrotron source (SAXS setup 3 described in the Experimental Section).[13] Here, the experiment could be conducted in a standard reaction vessel under stirring. The colloidal solution is continuously pumped through Teflon tubings from the reaction vessel to a nozzle where the X-ray beam is focused. The time span from the extraction to the measurement is typically in the range of several seconds. This setup was developed for time-resolved *in situ* SAXS studies of nanoparticle growth processes that proceed on a time scale of several minutes to hours. It offers a container-less measurement combined with a high time resolution necessary to obtain the demanded *in situ* information about the nanoparticle growth. From each scattering curve, the average radius, polydispersity, relative volume fraction (directly proportional to the total volume of all particles), and relative number of particles are available. The size distribution is assumed to be a Schulz-Zimm distribution. Selected scattering curves and their corresponding theoretical fits can be found in the Supporting Information S5a.

In Figure 5a—c, the results of the mathematical modeling of the scattering curves are displayed. At the first data point (2 min), the SAXS results show unambiguously very small particles with broad size distribution ($R_{avg} \sim 1$ nm, polydispersity $\sim 60\%$) (see Figure 5a). Within the next 40 min, the evaluation of the subsequent scattering curves yields no significant change besides an increase in the number of particles and thus of the volume fraction, as well. The SP-2 is observed at around 85 min. At this time, the corresponding scattering curves change significantly (see Supporting Information S5b).

The examined average particle radius increases to 5.2 nm, while the polydispersity decreases to around 15% within approximately 2 min. The volume fraction, before and after the SP-2, remains the same, whereas the number of particles drops down to 1/80 of the former amount. Thus, the growth of the particles is again accompanied by a decrease of the particle concentration. The synthesized Ag-NPs are stable after the SP-2 with a mean radius of about 5—7 nm and a narrow size distribution (polydispersity about 15%). In comparison to the synthesis without PVP as steric stabilizer (Ag-System 1), it can be assumed that the reduction process is not affected and occurs on a similar time scale (<1 s). Thus, the reduction process is again separated from the actual growth.

Nanoparticle Growth Mechanism Deduced for Ag-System 2. The experimental results lead to an interpretation of a growth mechanism consisting of four steps. These four steps are actually the same as deduced for Ag-System 1 (see Figure 6). The first step incorporates the immediate chemical reduction of the silver salt. The second step is the first coalescent process, leading to

a)

b)

c)
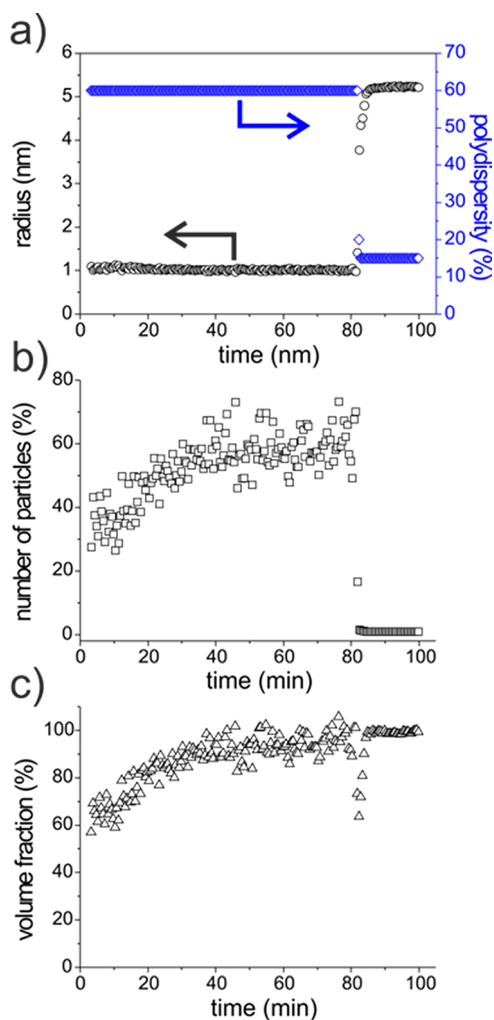
Figure 5. Evaluation of the SAXS data on the formation of silver nanoparticles (Ag-NPs) as a function of reaction time using a free liquid jet: (a) mean radius and polydispersity, (b) normalized number of particles (normalized to 1 at the last data point), and (c) volume fraction (normalized to 100 at the last data point).

an ensemble of particles having a mean radius of approximately 1 nm and a polydispersity of around 60%. The high polydispersity documents the existence of a notable amount of particles with radii between 2 and 5 nm, corresponding to a plasmon resonance at around 390 nm. On the basis of the SAXS measurement, this second step occurs within the first 2 min, whereby the UV−vis data indicate that this step occurs within the first seconds after mixing the reactants. The third step of the growth is a metastable state of these nanoparticles, with a mean radius of 1 nm. The metastable state lasts for about 30−90 min. In that period, no substantial change was detected with either SAXS or UV−vis. The fourth (final) step is the coalescence of the present particles, which occurs within 2−3 min. The coalescence stops when the particles reach a size at which the colloidal stability is sufficient to prevent aggregation and coalescence. It is again the most probable consequence of an almost constant volume

fraction together with increasing mean radius (from 1.2 to 5.2 nm), accompanied by a significant decrease of the particle concentration (see Figure 5). Effectively, on average, almost 100 particles merge to form a new stable nanoparticle in this step (number of particles decreases to approximately 1/80 of the former amount). This is also supported by the SEM experiments which show aggregated particles only for samples prepared during the SP-2 (see Figure 4c).

In conclusion, the claimed growth mechanism of Ag-System 2 consists of two distinct processes of coalescence (step 2 and 4), as deduced for Ag-System 1.

Comparison of the Growth Mechanisms. The aim of this contribution is to address two important issues in colloidal science: (i) the analogies and differences between nanoparticle growth processes of different elements such as gold and silver and (ii) the influence of a steric stabilizing agent on the growth process.

Comparing the results of the two Ag-NP systems and of the corresponding Au-NP synthesis[14] reveals similarities and analogies but also differences. The obvious similarity is that the particle growth mechanisms from the Au-NP system and the two Ag-NP systems consist of a growth due to coalescence. A process of coalescence demands a process of aggregation, which is the consequence of an insufficient colloidal stability. Thus, the actual particle growth is governed by the colloidal stability which appears to be a fundamental principle of metal nanoparticle growth. The main difference between the growth mechanisms of the Au and Ag systems is that the Au-NP growth consists solely of one step of coalescence. This step proceeds within the first 2−5 s after mixing the reactants, whereas the growth of the two Ag-NP systems consists of two distinct coalescent processes. However, the first two steps of all systems are the same (see Figure 6): reduction followed by a fast growth due to coalescence. After these two steps, the mean radius of the Ag-System 1 and the Au-NP system is around 2−3 nm. The particles of Ag-System 2, at which PVP is added, are the smallest with a mean radius of 1 nm. It should be noted that the polydispersity at this point of the reaction is much higher in both Ag-NP systems than in the Au-NP system (50% compared to 15−20%). The second coalescent step of Ag-System 1 after a metastable phase originates from a decrease of electrostatic stabilization.

This change of electrostatic stability is most likely correlated with the hydrolysis of borohydride. A detailed study of this hydrolysis was done by Gardiner *et al*. They specified that in water the borohydride species is converted into alkaline tetrahydroxyborate ions, accompanied by hydrogen evolution.[26] Although extensively studied, the exact hydrolysis mechanism leading to $B(OH)_4^-$ remains rather speculative.[28] More than 40 years ago, $BH_3(OH)^-$ was identified as a short
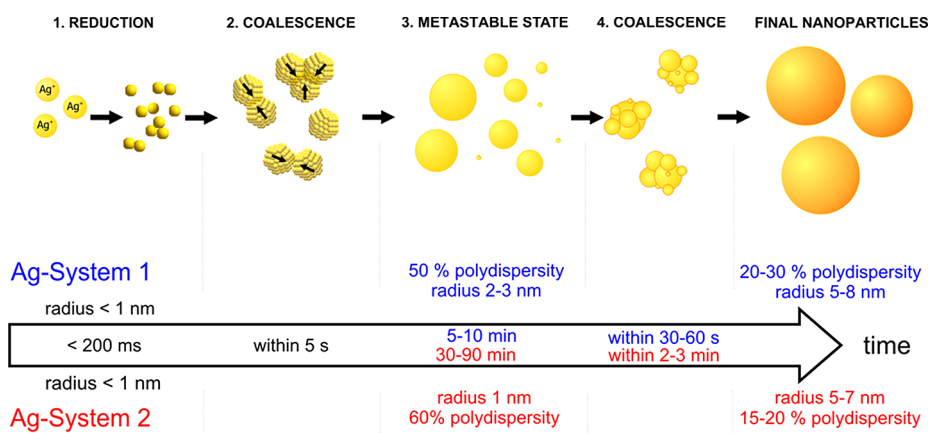
Figure 6. Schematic illustration of the deduced four-step growth mechanism deduced for both Ag-NP systems.

living intermediate.[26,29] Even today, this borate species remains the only one besides $B(OH)_4^-$ that was detected during the hydrolysis process.[27] Nevertheless, the reaction must occur stepwise, with the intermediates $BH_2(OH)_2^-$ and $BH(OH)_3^-$ being short living species.[27] Numerous studies also described that the reaction is accelerated in the presence of metal NPs.[30] The consequence of the hydrolysis is an increase of the pH from about 9 to 11. In addition, the ratio of $BH_4^-/B(OH)_4^-$ decreases due to an increasing $B(OH)_4^-$ concentration. Thus, the decrease of stability could be driven by a changing ratio of $BH_4^-/B(OH)_4^-$, the increasing pH, or a combination of both.

The exact nature of the change from the Ag-NP surface/electrolyte interface is difficult to determine. Nevertheless, the observed sudden coalescent process of all particles demands a destabilization of particles of different sizes, due to the relatively high polydipsersity before the switching point of both Ag-NP systems. This can hardly be explained by a change of ionic strength since both anions (BH_4^- and $B(OH)_4^-$) are monovalent, the overall salt concentration remains constant, and intermediate species are more or less not present.[31] The pH value is known to have an influence on the zeta-potential for metal-oxide nanoparticles due to the protonation and deprotonation of surface adsorbates. For a (noble) metal such as silver, one would not expect that the surface charge and hence the surface potential is strongly dependent on the pH value. Nevertheless, even for a pristine gold surface, it was shown *via* AFM force distance measurements that the pH as well as the counterions can influence the electric double layer.[31] Even a point of zero charge at a pH value of around 5 was deduced. However, the surface chemistry of the pristine colloidal silver/electrolyte interface with different concentrations of borohydride/tetrahydroxyborate at different pH values is, to the best of our knowledge, not discussed in the literature. Therefore, the exact nature of the stability decrease at the switching point is very speculative but is most likely correlated with any change of the Ag-NP surface, probably due to an

adsorption of borate species. In addition, this change of stability is obviously size-dependent since particles with radii of approximately 3 nm are not stable but those with radii of 5−8 nm are stable. When comparing Ag-System 1 with the corresponding gold system (reduction of $HAuCl_4$ with $NaBH_4$),[14] it becomes evident that the Au-NP surface chemistry is not affected by the hydrolysis of $NaBH_4$, whereas the colloidal silver surface is affected. As a result, the Au-NP formation process is relatively simple, and the synthesis is reproducible and easy to handle. In contrast, the synthesis of Ag-System 1 proceeds by a more complex process, which is strongly dependent on the mixing conditions. As a result, reproducibility in terms of particle size and polydispersity is hard to control (see Supporting Information S1).

Adding PVP to the synthesis and thus "additional colloidal stability" does not change the growth mechanism, but the beforehand mentioned difficulties can be controlled. With PVP, the synthesis is reproducible and reveals long-term stable final particles with a mean radius of about 5−7 nm at a polydispersity of approximately 15−20%. However, two major questions arise when comparing the two Ag-NP syntheses: (1) Why is the metastable phase much longer when using PVP, and (2) why does the four-step growth mechanism with two distinct processes of coalescence still persist when PVP is added?

The longer metastable phase can be related to a decelerated hydrolysis, if connecting the change of the surface chemistry (decrease of stability) at the switching point with the hydrolysis. In this context, the longer duration of the metastable phase would not be surprising considering that hydrolysis is accelerated in the presence of metal nanoparticles[27,32,33] and that it is also well-known that polymers (in particular PVP) adsorbed at the particle surface can decrease the catalytic activity.[34] The difference of the hydrolysis kinetic between Ag-System 1 and 2 can be investigated with a facile experiment by using $HAuCl_4$ as an indicator for residual BH_4^-.

When gold salt is added to the colloidal silver solution, Au(III) is reduced immediately if sufficient

BH$_4^-$ is left. As a result, Au-NPs with a strong absorbance in the 500 nm region are formed. Even small amounts of Au-NPs can be detected with UV−vis spectroscopy. In addition, if insufficient BH$_4^-$ is left to reduce most of the gold salt, the trivalent gold ions will decrease the colloidal stability substantialy, which leads to an aggregation of the Ag-NP. This can be detected with UV−vis, as well. The experimental findings (see Supporting Information S6) reveal unambiguously that the hydrolysis in Ag-System 2 is slower than that in Ag-System 1 and that the conversion of BH$_4^-$ to B(OH)$_4^-$ proceeds during the entire metastable phase.

The second question is not as trivial as it might appear. Especially because little is known about the mechanism of steric stabilization and even less about the combination with electrostatic stabilization.[19] It becomes even more complicated as the actual origin of the change in surface chemistry at the SP-1 remains speculative even for Ag-System 1. However, the gained mechanistic understanding reveals important information how PVP affects the Ag-NP growth.

At first, the particles of Ag-System 2 (with PVP) are smaller than those in Ag-System 1 after each step of coalescence. Consequently, the overall colloidal stability increases when adding PVP to the system. Initially, this is probably not surprising but is in fact far from being self-evident. The effect of PVP (which adsorbs at the particle's surface) on the electric double layer of the silver colloids is neither predictable nor thoroughly investigated. Therefore, it could also lead to a decrease of colloidal stability.[19]

Even if PVP is added, the particle stability decreases tremendously before the SP-1, leading to the second step of coalescence. As stated before, this is most likely connected to the hydrolysis and thus to the ratio of BH$_4^-$/B(OH)$_4^-$. The process that leads to the tremendous change of the nanoparticle surface chemistry in Ag-System 1 occurs also in the presence of adsorbed PVP. This implies that although the colloidal stability in Ag-System 2 is a combination of electrostatic and steric stabilization, the driving force for the particle growth is still the electrostatic stabilization.

The result of this contribution is that for the investigated nanoparticle syntheses (Au[14] and Ag) with NaBH$_4$ as reducing agent, the growth is only governed by coalescence, even after the addition of a steric stabilizing agent. As already stated, a process of coalescence demands a process of aggregation which is the result of insufficient particle stability. In addition, the use of strong reducing agents such as NaBH$_4$ results in a reduction faster than the actual growth (few milliseconds *vs* several seconds). Consequently, the particle growth and thus the final size distribution is only governed by the particle stability and independent from any kind of classical or nonclassical nucleation process.

CONCLUSIONS

The growth process of Ag-NP synthesized by the chemical reduction of AgClO$_4$ using NaBH$_4$ as reducing agent is only due to coalescence. This finding is in accordance with the mechanism derived for the corresponding Au-NP system comprising the same reducing agent.[14] Accordingly, the principle of growth of these silver and gold nanoparticle syntheses is the same.

However, the difference between the Au-NP and Ag-NP formation is that the growth mechanism of the Au-NP consists of only one process of coalescence that proceeds within a few seconds after mixing the reactants, whereas the Ag-NP growth proceeds in two distinct processes of coalescence. The first is similar to the Au-NP system. The second is most likely the consequence of a change of surface chemistry of the NP due to the hydrolysis of BH$_4^-$ species. In contrast, the surface chemistry of the Au-NP is not affected by the hydrolysis.

The addition of a further steric stabilizing agent (Ag-System 2) does not principally affect the growth mechanism. It only modifies the duration of each step. These results suggest that for syntheses of colloidal metal nanoparticles at which the monomer-supplying chemical reaction is faster than the actual growth, coalescence and thus also aggregation is a fundamental principle of nanoparticle growth.

EXPERIMENTAL SECTION

Ag-NP Syntheses. *Ag-System 1:* All experiments were performed at room temperature (23 °C) under ambient conditions in Erlenmeyer flasks or beakers which were cleaned with concentrated nitric acid and rinsed in copious amounts of purified water before use. The Ag-NP synthesis was adapted from a synthesis routine described by Van Hyning *et al.*[15−17] To investigate the growth process with time-resolved methods, the synthesis was adjusted to obtain a mixing ratio of 1:1 of the aqueous metal salt and reducing agent solutions, with final concentrations of 0.25 mM AgClO$_4$·H$_2$O (99.9%, Sigma Aldrich) and 1.5 mM NaBH$_4$ (97%, Roth), respectively. Solutions were prepared using purified water (18.2 MΩ·cm Milli-Q, Millipore).

In brief, 22.53 mg of AgClO$_4$·H$_2$O was dissolved in 200 mL of H$_2$O (0.5 mM), and 22.7 mg of NaBH$_4$ was dissolved in 200 mL of H$_2$O (3.0 mM). The NaBH$_4$ solution is not stable due to reaction

of borohydride with water. The reaction takes about 6 h to reach a conversion of 50%, depending on the temperature, the surface of the solution (thus dependent on the reaction vessel), and stirring.[30] For each experiment, the solution was freshly prepared to avoid any influence of NaBH$_4$ concentration changes. In addition, the synthesis is strongly dependent on the mixing conditions. Therefore, local fluctuation of the BH$_4^-$ and Ag$^+$ ion concentration due to non-uniform mixing leads to a very broad range of particle sizes and thus high polydispersities. However, a study of the influence of mixing conditions is not the aim of this work.

Ag-System 2: All experiments were performed at room temperature (around 23 °C) under ambient conditions in Erlenmeyer flasks. The flasks were first cleaned with concentrated nitric acid and rinsed in copious amounts of purified water. Solutions were

prepared using purified water (18.2 MΩ·cm Milli-Q, Millipore). Sodium borohydride was purchased from Roth (>97%), poly-(vinylpyrrolidone) (PVP) from Alfa-Aesar (58 000 MW avg), and silver perchlorate monohydrate from Sigma Aldrich (>99.9). The two solutions were freshly prepared before each experimental run and were mixed in a ratio of 1:2. In a typical experiment, 85 mg of $NaBH_4$ was dissolved in 0.5 L of water (4.5 mM); in the second flask, 62 mg of PVP (1.1×10^{-3} mM) and 85 mg of $AgClO_4 \cdot H_2O$ (0.375 mM) were dissolved in 1.0 L of water. The final $AgClO_4$ and $NaBH_4$ concentrations are again 0.25 and 1.5 mM, respectively.

In Situ SAXS. The Ag-System 1 was studied with time-resolved SAXS using a conventional lab-scale instrument (SAXSess, Anton Paar GmbH, Graz, Austria). To achieve a higher time resolution (necessary for the investigation of the first seconds of the growth process), a continuous flow setup (CFS) was combined with the instrument. The setup is referred to as *SAXS setup 1* in this contribution. The basic principle of this setup is the transformation of the time scale into a length scale (for detailed information of that method and setup, see ref 14). Thus, the CFS offers a millisecond time resolution, though the actual time resolution of the SAXS measurement is on the order of seconds to minutes. Teflon tubes of different lengths represent different points of time in the reaction. When this setup was applied for Ag-System 1, no aggregation (therefore no important influence) of the colloids in solution was observed in the first 2−3 s, although the solution is not stirred in the CFS. At longer durations (>3−4 s) and when a Teflon tubing with an inner diameter of >1 mm was used, large aggregates were detected, indicating unwanted influence on the growth process. In this setup, Ag-NPs were prepared by the homogeneous mixing of the two aqueous solutions, applying a self-manufactured Teflon Y-mixer. The online characterization of this fast process (2 s) was enabled by coupling the Y-mixer operating in continuous-flow mode with a conventional SAXS instrument. The two solutions (aqueous solutions of silver salt and reducing agent) were mixed, and using several tube lengths, a SAXS measurement was performed. The Teflon tubing, flow capillary, and glassware were cleaned with concentrated nitric acid, water, and isopropyl alcohol prior to each experimental run. The successful cleaning of the SAXS capillary was confirmed by recording a scattering curve of ultrapure deionized water.

The further particle growth (>30 s) was investigated conventionally by extracting successively small amounts of the batch solution and inserting them in the flow cell of the SAXS instrument (SAXSess, Anton Paar GmbH). The setup is referred to as *SAXS setup 2*. To avoid alteration of the sample during SAXS measurement, each extracted sample was mixed in a ratio of 4:1 with PVP (6.5×10^{-4} mM) dissolved in water. The time delay between the extraction and the actual measurement was below 5 s.

The Ag-System 2 was investigated using another recently presented SAXS setup[13] that couples the size-controlled synthesis of nanoparticles in standard reaction vessels to synchrotron-based SAXS *via* a free liquid jet. The setup is referred to as *SAXS setup 3*. The technique offers the unique possibility to follow the complete nanoparticle growth process *in situ*, right from the beginning, for hours, with a time resolution that depends only on the photon flux and the acquisition time of the detector but not on sample exchange procedures. Moreover, capillary effects such as the contamination at the wall of the sample cell are prevented. Thus, a quantitative time-resolved analysis of the small particles formed in the initial stage of the synthesis reaction is enabled.

Evaluation of SAXS Data. The scattering curves of the colloidal solution were analyzed assuming spherical shape, a homogeneous electron density, and a Schulz-Zimm size distribution. The assumption is supported by the UV−vis, SEM, and TEM investigation shown in Figure 2a−d.

The Schulz-Zimm distribution is given by

$$f(r) = (z+1)^{z+1} x^2 \frac{\exp[-(z+1)x]}{R_{avg} \Gamma(z+1)} \tag{1}$$

where R_{avg} is the mean radius, $x = r/R_{avg}$, z is related to the polydispersity p ($p = \sigma/R_{avg}$) by $z = 1/p^2 - 1$, and σ^2 is the variance of the distribution. The mean particle volume can be

calculated from the third moment of the size distribution leading to

$$\langle V \rangle = \frac{4\pi}{3}\langle R \rangle^3 = \frac{4\pi}{3}\langle R_{avg} \rangle^3 \frac{(z+3)(z+2)}{(z+1)^2}$$

with z defined as above.

The scattering intensity of non-aggregated particles can be assumed to be proportional to the form factor of a single particle $P(q)$. Thus, the scattering intensity of monodisperse spheres with homogeneous electron density with volume V_{part} is given by

$$I(q) = NI_{part}(q) = NV_{part}^2 P(q) = N4\pi V_{part}^2$$
$$= \left[\Delta\rho \frac{3(\sin(qR) - qR\cos(qR))}{qR} \right]^2 \tag{2}$$

In the case of polydisperse spherical particles, one has to sum the scattering intensities over all particle sizes weighted by their frequency or to integrate using a size distribution function. It is common to use the Schulz-Zimm distribution for polydisperse particles. Hence, the scattering intensity is given by

$$I(q) = N \int_0^\infty f(r) V_{part}^2 P(q) dr \tag{3}$$

An analytical solution of that integral can be found in Kotlarchyk *et al.*[35] In order to analyze the nucleation and growth mechanism of nanoparticles, the number of particles is important. This information can be obtained by using the general relation of $I(q = 0)$ for a single particle, which is independent of its shape and size, that is, $I = (\Delta\rho)^2 V^2$. Thus, the scattered intensity $I(q = 0)$ of polydisperse particles can be written as

$$I(q) = N\langle V^2 \rangle (\Delta\rho)^2 \tag{4}$$

where N is the number of particles and $\langle V^2 \rangle$ the mean value of V^2. Due to the overlapping of the scattering intensity with the primary beam, $I(q = 0)$ cannot be measured directly but is accessible *via* the extrapolation of $I(q)$ for $q \rightarrow 0$.

The polydispersity for the mathematical modeling of the scattering curves derived from the CFS experiment was kept constant at a value of 50% since it only differs slightly (±5%). A better determination would demand a higher signal-to-noise ratio. Selected scattering curves and their corresponding fits (model function) for both Ag-NP systems are given in the Supporting Information (S1 and S2).

In Situ UV−Vis Spectroscopy. The UV−vis spectra were recorded on an AvaSpec-2048TEC-2 equipped with a deuterium halogen light source (Avantes, Broomfield, USA), connected to a 10 mm optical path length cuvette holder *via* fiber optical cables. The UV−vis investigations of the Ag-NPs were carried out in a standard 1 mL UV cuvette enabling the stirring of the solution.[36] The time resolution was about 250 ms. The first data point was acquired after approximately 500 ms due to the mixing time. To receive data for the Ag-System 1 after the first 80 s, the synthesis was performed outside the cuvette as hydrogen evolution due to hydrolysis of sodium borohydride becomes dominant and precludes UV−vis measurements. Samples of 100 μL were extracted and mixed with 400 μL in water dissolved PVP (6.5×10^{-4} mM) to avoid agglomeration/aggregation. The time delay between the extraction and the actual measurement was below 5 s.

***Ex Situ* Characterization of the Ag-NP.** The final Ag-NP were investigated with SEM and TEM. The SEM imaging was performed on a JEOL JSM-7401F (Hitachi Ltd., Tokyo, Japan) with an acceleration voltage of 10 kV at a working distance of 8 mm. The TEM imaging was performed with a Zeiss LIBRA 200-FE instrument (Zeiss, Germany) operating at 200 kV. Ag-System 1: To avoid aggregation of the final NP during the SEM/TEM sample preparation, 100 μL of the final colloidal solution was spin-coated onto the wafer/grid. As a result, the drying process lasted less than 1 s but only a few single nanoparticles were observed in the TEM and SEM investigations, which do not allow the determination of a size distribution (no statistic available). Ag-System 2: For the SEM and TEM sample preparation, 100 and 10 μL,

respectively, of the solution were deposited on the wafer/grid and immediately removed using an Eppendorf pipet. For the TEM sample preparation, 10 μL of the solution was dropped on the TEM grid and immediately removed with an Eppendorf pipet.

REFERENCES AND NOTES

1. Storhoff, J. J.; Elghanian, R.; Mucic, R. C.; Mirkin, C. A.; Letsinger, R. L. One-Pot Colorimetric Differentiation of Polynucleotides with Single Base Imperfections Using Gold Nanoparticle Probes. *J. Am. Chem. Soc.* **1998**, *120*, 1959–1964.
2. Bond, G. C.; Louis, C.; Thompson, D. T. *Catalysis by Gold*; Imperial College Press: London, 2006; Vol. 6.
3. Faraday, M. The Bakerian Lecture: Experimental Relations of Gold (and Other Metals) to Light. *Philos. Trans. R. Soc. London* **1857**, *147*, 145–181.
4. Finney, E. E.; Finke, R. G. Nanocluster Nucleation and Growth Kinetic and Mechanistic Studies: A Review Emphasizing Transition-Metal Nanoclusters. *J. Colloid Interface Sci.* **2008**, *317*, 351–374.
5. Lamer, V. K.; Dinegar, R. H. Theory, Production and Mechanism of Formation of Monodispersed Hydrosols. *J. Am. Chem. Soc.* **1950**, *72*, 4847–4854.
6. Zheng, H. M.; Smith, R. K.; Jun, Y. W.; Kisielowski, C.; Dahmen, U.; Alivisatos, A. P. Observation of Single Colloidal Platinum Nanocrystal Growth Trajectories. *Science* **2009**, *324*, 1309–1312.
7. Biswas, K.; Varghese, N.; Rao, C. N. R. Growth Kinetics of Gold Nanocrystals: A Combined Small-Angle X-ray Scattering and Calorimetric Study. *Small* **2008**, *4*, 649–655.
8. Buhro, W. E.; Richards, V. N.; Rath, N. P. Pathway from a Molecular Precursor to Silver Nanoparticles: The Prominent Role of Aggregative Growth. *Chem. Mater.* **2010**, *22*, 3556–3567.
9. Pemberton, J. E.; Huang, Y. Synthesis of Uniform, Spherical Sub-100 nm Silica Particles Using a Conceptual Modification of the Classic LaMer Model. *Colloids Surf., A* **2010**, *360*, 175–183.
10. Nagy, J. B.; Destree, C. Mechanism of Formation of Inorganic and Organic Nanoparticles from Microemulsions. *Adv. Colloid Interface Sci.* **2006**, *123*, 353–367.
11. Polte, J.; Ahner, T. T.; Delissen, F.; Sokolov, S.; Emmerling, F.; Thunemann, A. F.; Kraehnert, R. Mechanism of Gold Nanoparticle Formation in the Classical Citrate Synthesis Method Derived from Coupled *In Situ* XANES and SAXS Evaluation. *J. Am. Chem. Soc.* **2010**, *132*, 1296–1301.
12. Polte, J.; Emmerling, F.; Radtke, M.; Reinholz, U.; Riesemeier, H.; Thunemann, A. F. Real-Time Monitoring of Copolymer Stabilized Growing Gold Nanoparticles. *Langmuir* **2010**, *26*, 5889–5894.
13. Polte, J.; Erler, R.; Thunemann, A. F.; Emmerling, F.; Kraehnert, R. SAXS in Combination with a Free Liquid Jet for Improved Time-Resolved *In Situ* Studies of the Nucleation and Growth of Nanoparticles. *Chem. Commun.* **2010**, *46*, 9209–9211.
14. Polte, J.; Erler, R.; Thunemann, A. F.; Sokolov, S.; Ahner, T. T.; Rademann, K.; Emmerling, F.; Kraehnert, R. Nucleation and Growth of Gold Nanoparticles Studied *via In Situ* Small Angle X-ray Scattering at Millisecond Time Resolution. *ACS Nano* **2010**, *4*, 1076–1082.
15. Van Hyning, D. L.; Klemperer, W. G.; Zukoski, C. F. Silver Nanoparticle Formation: Predictions and Verification of the Aggregative Growth Model. *Langmuir* **2001**, *17*, 3128–3135.
16. Van Hyning, D. L.; Klemperer, W. G.; Zukoski, C. F. Characterization of Colloidal Stability during Precipitation Reactions. *Langmuir* **2001**, *17*, 3120–3127.
17. Van Hyning, D. L.; Zukoski, C. F. Formation Mechanisms and Aggregation Behavior of Borohydride Reduced Silver Particles. *Langmuir* **1998**, *14*, 7034–7046.
18. Grubbs, R. B. Roles of Polymer Ligands in Nanoparticle Stabilization. *Polym. Rev.* **2007**, *47*, 197–215.
19. Finke, R. G.; Ott, L. S.; Hornstein, B. J. A Test of the Transition-Metal Nanocluster Formation and Stabilization Ability of the Most Common Polymeric Stabilizer, Poly-(vinylpyrrolidone), as Well as Four Other Polymeric Protectants. *Langmuir* **2006**, *22*, 9357–9367.
20. ISO, International Organization for Standardization: ISO/TS 27687:2008(E), **2008**
21. Kelly, K. L.; Coronado, E.; Zhao, L. L.; Schatz, G. C. The Optical Properties of Metal Nanoparticles: The Influence of Size, Shape, and Dielectric Environment. *J. Phys. Chem. B* **2003**, *107*, 668–677.
22. Sun, Y. G.; Xia, Y. N. Gold and Silver Nanoparticles: A Class of Chromophores with Colors Tunable in the Range from 400 to 750 nm. *Analyst* **2003**, *128*, 686–691.
23. Sonnichsen, C.; Franzl, T.; Wilk, T.; von Plessen, G.; Feldmann, J. Plasmon Resonances in Large Noble-Metal Clusters. *New J. Phys.* **2002**, *4*, DOI: 10.1088/1367-2630/4/1/393.
24. Abecassis, B.; Testard, F.; Spalla, O.; Barboux, P. Probing *In Situ* the Nucleation and Growth of Gold Nanoparticles by Small-Angle X-ray Scattering. *Nano Lett.* **2007**, *7*, 1723–1727.
25. Bolze, J.; Peng, B.; Dingenouts, N.; Panine, P.; Narayanan, T.; Ballauff, M. Formation and Growth of Amorphous Colloidal $CaCO_3$ Precursor Particles As Detected by Time-Resolved SAXS. *Langmuir* **2002**, *18*, 8364–8369.
26. Gardiner, J. A.; Collat, J. W. Hydrolysis of Sodium Tetrahydroborate. Identification of Intermediate. *J. Am. Chem. Soc.* **1964**, *86*, 3165–3166.
27. Demirci, U. B.; Andrieux, J.; Hannauer, J.; Gervais, C.; Goutaudier, C.; Miele, P. Spontaneous Hydrolysis of Sodium Borohydride in Harsh Conditions. *Int. J. Hydrogen Energy* **2011**, *36*, 224–233.
28. Rostamikia, G.; Janik, M. J. Direct Borohydride Oxidation: Mechanism Determination and Design of Alloy Catalysts Guided by Density Functional Theory. *Energy Environ. Sci.* **2010**, *3*, 1262–1274.
29. Gardiner, J. A.; Collat, J. W. Kinetics of Stepwise Hydrolysis of Tetrahydroborate Ion. *J. Am. Chem. Soc.* **1965**, *87*, 1692–1694.
30. Andrieux, J.; Swierczynski, D.; Laversenne, L.; Garron, A.; Bennici, S.; Goutaudier, C.; Miele, P.; Auroux, A.; Bonnetot, B. A Multifactor Study of Catalyzed Hydrolysis of Solid $NaBH_4$ on Cobalt Nanoparticles: Thermodynamics and Kinetics. *Int. J. Hydrogen Energy* **2009**, *34*, 938–951.
31. Kleijn, J. M.; Giesbers, M.; Stuart, M. A. C. The Electrical Double Layer on Gold Probed by Electrokinetic and Surface Force Measurements. *J. Colloid Interface Sci.* **2002**, *248*, 88–95.
32. Metin, O.; Ozkar, S. Hydrogen Generation from the Hydrolysis of Sodium Borohydride by Using Water Dispersible, Hydrogenphosphate-Stabilized Nickel(0) Nanoclusters as Catalyst. *Int. J. Hydrogen Energy* **2007**, *32*, 1707–1715.
33. Metin, O.; Kocak, E.; Ozkar, S. Effect of Stabilizer Type on the Activity and Stability of Water-Dispersible Cobalt(0) Nanocluster Catalysts in Hydrogen Generation from the Hydrolysis of Sodium Borohydride. *React. Kinet. Mech. Catal.* **2011**, *103*, 325–340.
34. Ott, L. S.; Finke, R. G. Nanocluster Formation and Stabilization Fundamental Studies: Investigating "Solvent-Only" Stabilization en Route to Discovering Stabilization by the Traditionally Weakly Coordinating Anion BF_4^- Plus High Dielectric Constant Solvents. *Inorg. Chem.* **2006**, *45*, 8382–8393.

35. Kotlarchyk, M.; Chen, S. H. Analysis of Small-Angle Neutron Scattering Spectra from Polydisperse Interacting Colloids. *J. Chem. Phys.* **1983**, *79*, 2461–2469.

36. Haiss, W.; Thanh, N. T. K.; Aveyard, J.; Fernig, D. G. Determination of Size and Concentration of Gold Nanoparticles from UV−Vis Spectra. *Anal. Chem.* **2007**, *79*, 4215–4221.